Journal of Solid State Chemistry 181 (2008) 1943–1949

Contents lists available at ScienceDirect

Journal of Solid State Chemistry

journal homepage: www.elsevier.com/locate/jssc

Fabrication and luminescent properties of the core–shell structured $YNbO_4:Eu^{3+}/Tb^{3+}@SiO_2$ spherical particles

Piaoping Yang [a,b], Zewei Quan [a], Chunxia Li [a], Jun Yang [a], Huang Wang [a], Xiaoming Liu [a], Jun Lin [a,*]

[a] State Key Laboratory of Rare Earth Resource Utilization, Changchun Institute of Applied Chemistry, Chinese Academy of Sciences, Changchun 130022, PR China
[b] College of Material Science and Chemical Engineering, Harbin Engineering University, Harbin 150001, PR China

ARTICLE INFO

Article history:
Received 1 February 2008
Received in revised form
17 March 2008
Accepted 24 April 2008
Available online 4 May 2008

Keywords:
Core–shell
$YNbO_4$
Luminescence
Phosphors
Sol–gel

ABSTRACT

The core–shell structured $YNbO_4:Eu^{3+}/Tb^{3+}@SiO_2$ particles were realized by coating the $YNbO_4:Eu^{3+}/Tb^{3+}$ phosphors onto the surface of spherical silica via a sol–gel process. The obtained materials were characterized by means of X-ray diffraction (XRD), field emission scanning electron microscopy (FE-SEM), transmission electron microscopy (TEM), Fourier transform IR spectroscopy (FT-IR), photoluminescence (PL) spectra, and cathodoluminescence (CL) spectra. The results indicate that 600 °C annealed samples consist of amorphous silica core and crystalline $YNbO_4$:Re shell, having perfect spherical morphology with uniform size distribution. Upon excitation by UV or electron beam, these phosphors show the characteristic $^5D_0$–$^7F_{1-4}$ emission lines of Eu^{3+} and the characteristic $^5D_4$–$^7F_{3-6}$ emission lines of Tb^{3+}. The PL intensities of Eu^{3+} can be tuned by altering the annealing temperature and the coating number of $YNbO_4:Eu^{3+}$ layers.

1. Introduction

Recently, nano-scale core–shell structured particles have attracted much attention due to their potential applications in the filed of diagnostics, catalysis, photonic crystals, and pharmacology [1–5]. In general, the core–shell structured materials are defined by a core that is covered by a shell with different composition [6–10]. The morphology, structure, and composition of these particles can be tuned in a controllable manner to tailor their physicochemical properties [10–16]. So far, a large number of approaches have been employed for the fabrication of such core–shell structured materials, including layer-by-layer technique, sol–gel process, template directed self-assembly, and in situ polymerization [17–19]. For most of these procedures, the degree of surface coverage is usually low and the coating is far from uniformity. The sol–gel method provides a simple and effective process for preparing core–shell structured materials with uniform coverage [11].

Furthermore, the demand for high resolution and efficiency in phosphors for cathode ray tubes (CRTs) and field emissive displays (FEDs) has also promoted the development of phosphors [20]. Particularly, the phosphors with non-agglomerated, mono-disperse, and spherical morphology (0.5–2 μm) are of special interest because of their brighter cathodoluminescent performance, high definition, and much improved screen packing [21,22]. Many synthetic processes have been developed to control the size and distribution of phosphor particles, including fluxes precipitation and spray pyrolysis [23,24]. But the obtained phosphors are far from ideal morphology.

Silica particles can be controllably prepared from nanometer to micrometer size with spherical morphology [25,26]. A kind of core–shell structured phosphors can be realized by coating phosphor layer onto the surface of spherical silica [6,7]. As a well-known self-activated compound, $LnNbO_4$ presents a strong broad band under ultraviolet excitation, which makes it potential to develop new, efficient luminescent materials [27,28]. So far, no report has been found concerning the functionalization of spherical silica with $YNbO_4:Eu^{3+}/Tb^{3+}$ phosphors. Herein, the nanometer mono-disperse core–shell $YNbO_4:Eu^{3+}/Tb^{3+}@SiO_2$ phosphors were prepared via the Pechini sol–gel process. The structure, morphology, and luminescence of the obtained materials were investigated in detail.

2. Experimental section

The starting materials: Y_2O_3 (99.99%, Shanghai Yuelong Nonferrous Metals Ltd.), Eu_2O_3 (99.99%, Shanghai Yuelong Nonferrous Metals Ltd.), Tb_4O_7 (99.99%, Shanghai Yuelong Nonferrous Metals Ltd.), ammonium niobium oxalate, $C_{10}H_8N_2O_{33}Nb_2$ (A. R., Fluka), tetraethyl orthosilicate, $Si(OC_2H_5)_4$ (TEOS, A. R., Beijing Beihua Chemicals Co., Ltd.), NH_4OH (25%, A. R., Beijing Beihua

* Corresponding author.
E-mail address: jlin@ciac.jl.cn (J. Lin).

0022-4596/$ - see front matter © 2008 Elsevier Inc. All rights reserved.
doi:10.1016/j.jssc.2008.04.025

Chemicals Co., Ltd.), polyethylene glycol (PEG, $M_w = 10000$, A. R., Beijing Beihua Chemicals Co., Ltd.), HNO_3 (65%, A. R., Beijing Beihua Chemicals Co., Ltd.), C_2H_5OH (A. R., Beijing Beihua Chemicals Co., Ltd.), citric acid (A. R., Beijing Beihua Chemicals Co., Ltd.), ethylene glycol (EG, A. R., Beijing Beihua Chemicals Co., Ltd.) were used without further purification.

2.1. Synthesis of spherical silica core

The mono-disperse silica spheres with particle sizes of 300 nm were prepared by hydrolysis of tetraethyl orthosilicate (TEOS), in an alcohol medium in the presence of water and ammonia via a modified Stöber process [25]. This method yielded the colloidal solution of silica particles with a narrow size distribution in the nanometer range, and the particle size of silica depended on relative concentration of the reactants. In a typical process, 8.4 mL of TEOS, 18 mL of deionized H_2O, and 97.9 mL of NH_4OH were added into 75.7 mL of absolute ethanol and stirred at room temperature for 4 h, resulting in the formation of white silica colloidal suspension. The silica particles were centrifugally separated from the suspension and washed several times with ethanol.

2.2. Coating of SiO_2 cores with $YNbO_4:Eu^{3+}$ shells

The core–shell structured $YNbO_4:Eu^{3+}@SiO_2$ phosphors were prepared by coating $YNbO_4:Eu^{3+}$ phosphor on the surface of silica via a Pechini sol–gel process [6,7,29]. The doping concentration of Eu^{3+} was 5 mol% to that of Y^{3+} in $YNbO_4:Eu^{3+}$. Typically, 0.2145 g of Y_2O_3 and 0.0176 g of Eu_2O_3 was dissolved in HNO_3 under vigorous stirring, and the superfluous HNO_3 was driven off until the pH value of the solution reached between two and three. The as-prepared material was mixed with 0.87 g ammonium niobium oxalate, 20 ml water–ethanol ($V/V = 15/5$) solution containing 0.8406 g citric acid as a chelating agent for the metal ions, followed by the addition of 0.8 g of PEG as a cross-linking agent with a final concentration of 0.04 g/mL. The solution was stirred for 1 h to form a sol, then the silica particles were added with vigorous stirring. After the suspension was further stirred for another 3 h, the silica particles were separated by centrifugation. The as-made samples were dried at 100 °C for 1 h immediately. Then the dried samples were annealed to the desired temperature (500–900 °C) with a heating rate of 1 °C/min and held there for 3 h in air. In this way, the core–shell structured $YNbO_4:Eu^{3+}@SiO_2$ materials were obtained, and the whole process is shown in Scheme 1. For the purpose of comparison, the coating sol was evaporated to form powders treated in a similar process. The $YNbO_4:Tb^{3+}@SiO_2$ phosphors with the Tb^{3+} molar ratio of 5 mol % to that of Y^{3+} were fabricated in the same manner of preparing $YNbO_4:Eu^{3+}@SiO_2$.

2.3. Characterization

X-ray diffraction (XRD) patterns were examined on a Rigaku–Dmax 2500 V diffractometer using Cu$K\alpha$ radiation ($\lambda = 0.15405$ nm). FT-IR spectra were measured with a Perkin-Elmer 580B IR spectrophotometer using KBr pellet technique. The morphology of the as-prepared samples was inspected on a field emission scanning electron microscopy (FE-SEM, XL30, Philips) and transmission electron microscope (TEM) (FEI Tecnai G2 S–Twin). The UV–vis excitation and emission spectra were obtained on a Hitachi F–4500 spectrofluorimeter equipped with a 150 W xenon lamp as the excitation source (the excitation spectra are calibrated for the system responsivity). Luminescence decay curves were obtained from a Lecroy Wave Runner 6100 digital oscilloscope (1 GHz) using a 250 nm laser (pulse width = 4 ns, gate = 50 ns) as the excitation source (Continuum Sunlite OPO).

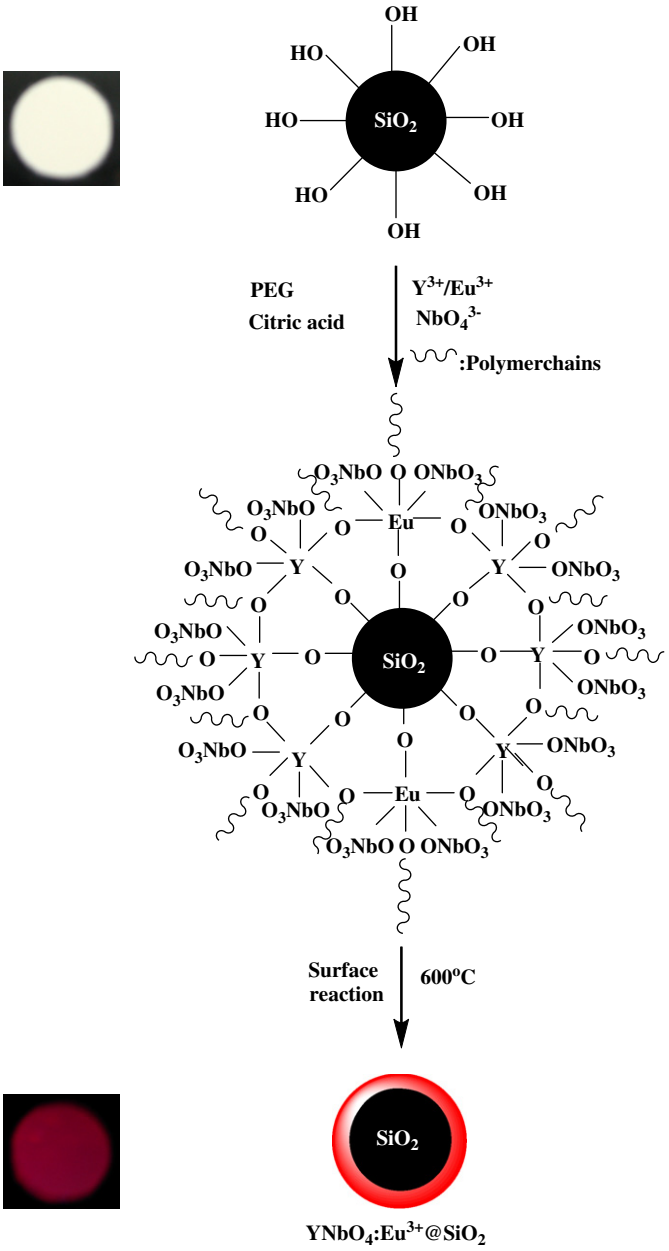

Scheme 1. Formation process of $YNbO_4:Eu^{3+}@SiO_2$ core–shell particles.

3. Results and discussion

3.1. Structure and morphology of $YNbO_4:Eu^{3+}/Tb^{3+}@SiO_2$ particles

Fig. 1A shows the XRD patterns for the 600 °C annealed $YNbO_4:Re@SiO_2$ composites, pure silica as well as the standard data for $YNbO_4$ (JCPDS No. 38-0187), respectively. As shown for $YNbO_4:Eu^{3+}@SiO_2$ (Fig. 1A(b)) and $YNbO_4:Tb^{3+}@SiO_2$ (Fig. 1A(c)), The diffraction peaks at $2\theta = 29.4°$ (112, strongest), 34.4° (200), 48.6° (204), and 58° (312) can be well indexed to the JCPDS Card 38–0187 for tetragonal $YNbO_4$, suggesting the successful crystallization of $YNbO_4$:Re on the surface of amorphous silica. The broad band peaking at $2\theta = 22°$ can be assigned to the characteristic

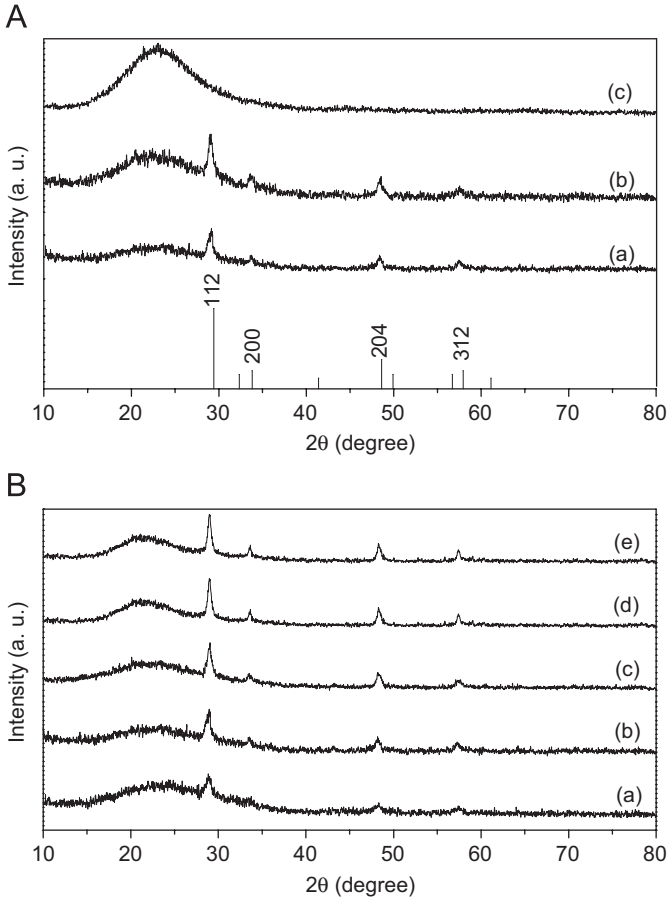

Fig. 1. X-ray diffraction patterns for (A) the 600 °C annealed $YNbO_4:Eu^{3+}@SiO_2$ (a), $YNbO_4:Tb^{3+}@SiO_2$ (b), pure SiO_2 (c), and the standard data for $YNbO_4$; (B) the $YNbO_4:Eu^{3+}@SiO_2$ particles annealed at 500 °C (a), 600 °C (b), 700 °C (c), 800 °C (d), and 900 °C (e).

diffraction for the amorphous SiO_2 cores (JCPDS 29–0085). Additionally, no other phase can be detected, indicating no other reaction occurs between silica (core) and the deposited phosphor (shell). Fig. 1B shows the XRD diffraction patterns of $YNbO_4:Eu^{3+}@SiO_2$ samples annealed from 500 to 900 °C. The XRD results indicate that the sample begins to crystallize in tetragonal $YNbO_4$ phase at 500 °C, and the crystallinity increases with the increase of annealing temperature. Furthermore, the nano-crystalline size of the crystallized phosphor can be calculated from the Scherrer formula [30]. The estimated average crystallite sizes of $YNbO_4:Eu^{3+}/Tb^{3+}$ in $YNbO_4:Eu^{3+}@SiO_2$ and $YNbO_4:Tb^{3+}@SiO_2$ are 13 and 15 nm, respectively. The XRD patterns reveal the structure of $YNbO_4:Eu^{3+}/Tb^{3+}$ belongs to the tetragonal crystal phase. And the refined crystallographic unit cell parameters and the calculated particle sizes for $YNbO_4:Eu^{3+}/Tb^{3+}@SiO_2$ annealed at 600 °C are list in Table 1.

Fig. 2 displays the SEM images of the pure SiO_2 particles, the pure $YNbO_4:Eu^{3+}$ powders, $YNbO_4:Eu^{3+}@SiO_2$, and $YNbO_4:Tb^{3+}@SiO_2$, respectively. It can be seen from Fig. 2(a) that pure SiO_2 consists of spherical particles with a uniform particle size of about 300 nm, and these particles are non-aggregated with narrow size distribution. While for the pure $YNbO_4:Eu^{3+}$ powders (Fig. 2(b)), irregular particles with size distribution from 150 to 500 nm are observed. The resulting $YNbO_4:Eu^{3+}/Tb^{3+}@SiO_2$ particles still keep the morphological properties of the silica particles, such as the spherical morphology, non-aggregation, and uniform size distribution. The results suggest that the coating of $YNbO_4:Eu^{3+}/Tb^{3+}$ has little

Table 1
Unit cell parameters and calculated sizes for $YNbO_4$ and those in the $YNbO_4:Eu^{3+}/Tb^{3+}@SiO_2$ core–shell particles annealed at 600 °C

Samples	*a* (nm)	*b* (nm)	*c* (nm)	Crystal size (nm)
$YNbO_4$	0.5164	0.5164	1.0864	
$YNbO_4:Eu^{3+}@SiO_2$	0.5179	0.5179	1.0851	13
$YNbO_4:Tb^{3+}@SiO_2$	0.5183	0.5183	1.0855	15

influence on the morphology of pure silica. The slightly larger particle size may be due to the deposited layer of phosphor on the surface of silica. Moreover, the irregular particles of the pure $YNbO_4:Eu^{3+}/Tb^{3+}$ powers cannot be observed in the resulting $YNbO_4:Eu^{3+}/Tb^{3+}@SiO_2$ particles (Fig. 2(c, d)), indicating the uniform coating of $YNbO_4:Eu^{3+}/Tb^{3+}$ onto the surface of silica particles.

The representative TEM images of the pure silica particles and the $YNbO_4:Eu^{3+}@SiO_2$ phosphors are depicted in Fig. 3, respectively. For the $YNbO_4:Eu^{3+}@SiO_2$ particles (Fig. 3(b)), the core–shell structure can be clearly observed because of the different electron penetrability between the cores and shells. The cores are black spheres with an average size of about 300 nm, which is similar to that of the pure SiO_2 particles (Fig. 3(a)), and the shell shows gray color with an average thickness of 30 nm. The HRTEM image was performed in the interface region of the core and shell for the $YNbO_4:Eu^{3+}@SiO_2$ particle as labeled in Fig. 3(b) and (c). As shown, the lattice fringes of crystalline phase ($YNbO_4$) can be seen clearly in Fig. 3(c). The distance (0.31 nm) between the adjacent two lattice fringes just matches well with the *d* (112) spacing (0.303 nm) of $YNbO_4$ (JCPDS 38-0187). The HRTEM result further confirms the crystalline $YNbO_4:Eu^{3+}$ on the surface of silica.

As shown in the IR spectrum for pure $YNbO_4:Eu^{3+}$ powders (Fig. 4(a)), a strong absorption peak at 810 cm^{-1} and a weak one at 452 cm^{-1} should be attributed to the internal modes of the tetrahedral NbO_4 unit [31]. For the pure silica (Fig. 4(b)), the absorption bands due to OH (3449 cm^{-1}), H_2O (1633 cm^{-1}), Si–O–Si (υ_s, 1100 cm^{-1}; υ_{as}, 810 cm^{-1}), Si–OH (υ_s, 951 cm^{-1}), and Si–O (δ, 470 cm^{-1}) (where υ_s represents symmetric stretching, υ_{as} asymmetric stretching, and δ bending) are obvious [6,7]. The strong bands of OH (3449 cm^{-1}) and H_2O (1633 cm^{-1}) suggest that a large number of OH groups and H_2O molecules present, which are essential for bonding metal ions from the coating sol and forming the phosphor layers on the silica surfaces. From the spectrum of the core–shell $YNbO_4:Eu^{3+}/Tb^{3+}@SiO_2$ sample (Fig. 4(c, d)), the absorption peaks of the NbO_4 unit or Si–O–Si (810 cm^{-1}) and the Si–O–Si bond (1110 cm^{-1}) for amorphous SiO_2 are observed clearly, and the weak peak of the NbO_4 unit (452 cm^{-1}) in $YNbO_4:Eu^{3+}$ disappears, which may attributed to the covering of the bending vibration of Si–O bond at 470 cm^{-1}. The intensity of OH groups from the as-formed silica particles have greatly been reduced in the 600 °C annealed $YNbO_4:Eu^{3+}/Tb^{3+}@SiO_2$ core–shell particles, which may be caused by the covering of –OH sites by the deposited phosphors.

3.2. Photoluminescence and cathodoluminescence properties

Fig. 5(a)–(d) shows the photoluminescence (PL) excitation and emission spectra of the $YNbO_4:Eu^{3+}@SiO_2$ and $YNbO_4:Tb^{3+}@SiO_2$ phosphors, respectively. In the excitation spectrum (monitored by the Eu^{3+} $^5D_0$–$^7F_2$ transition at 612 nm) for $YNbO_4:Eu^{3+}@SiO_2$ (Fig. 5(a)), the obtained excitation spectrum consists of a broad intense band with a maximum at 255 nm and some weak lines between 300 and 500 nm. The broad band with a maximum at 255 nm can be ascribed to the NbO_4^{3-} groups, and the weak lines arise from *f*–*f* transitions within the Eu^{3+} $4f^6$ electron configuration. The excitation lines can be assigned to $^7F_0 \rightarrow {}^5H_6$ (322 nm), $^7F_0 \rightarrow {}^5D_4$

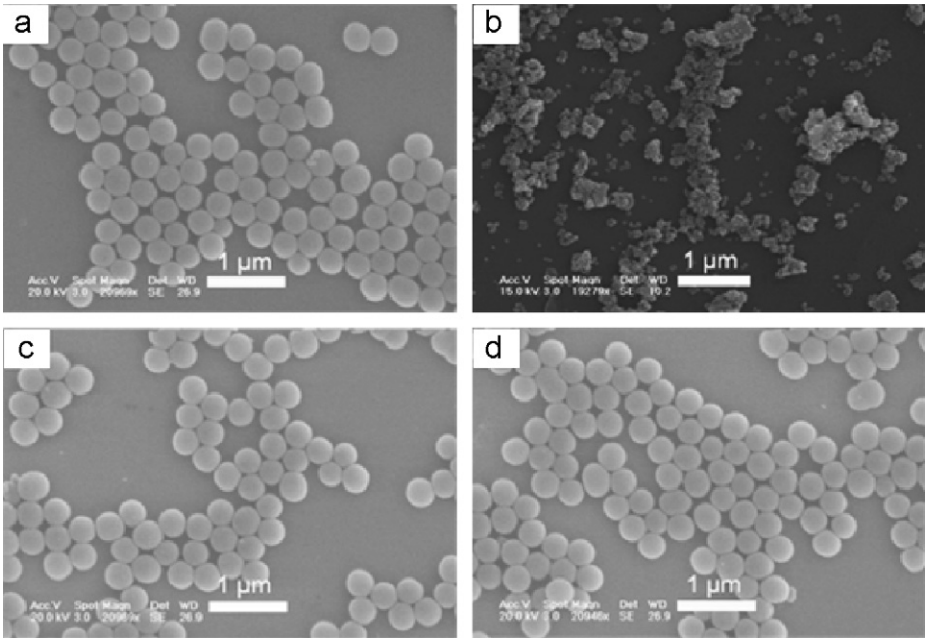

Fig. 2. SEM images for the 600 °C annealed pure SiO_2 (a), pure $YNbO_4$ powder (b), $YNbO_4$:Eu^{3+}@SiO_2 (c), and $YNbO_4$:Tb^{3+}@SiO_2 (d).

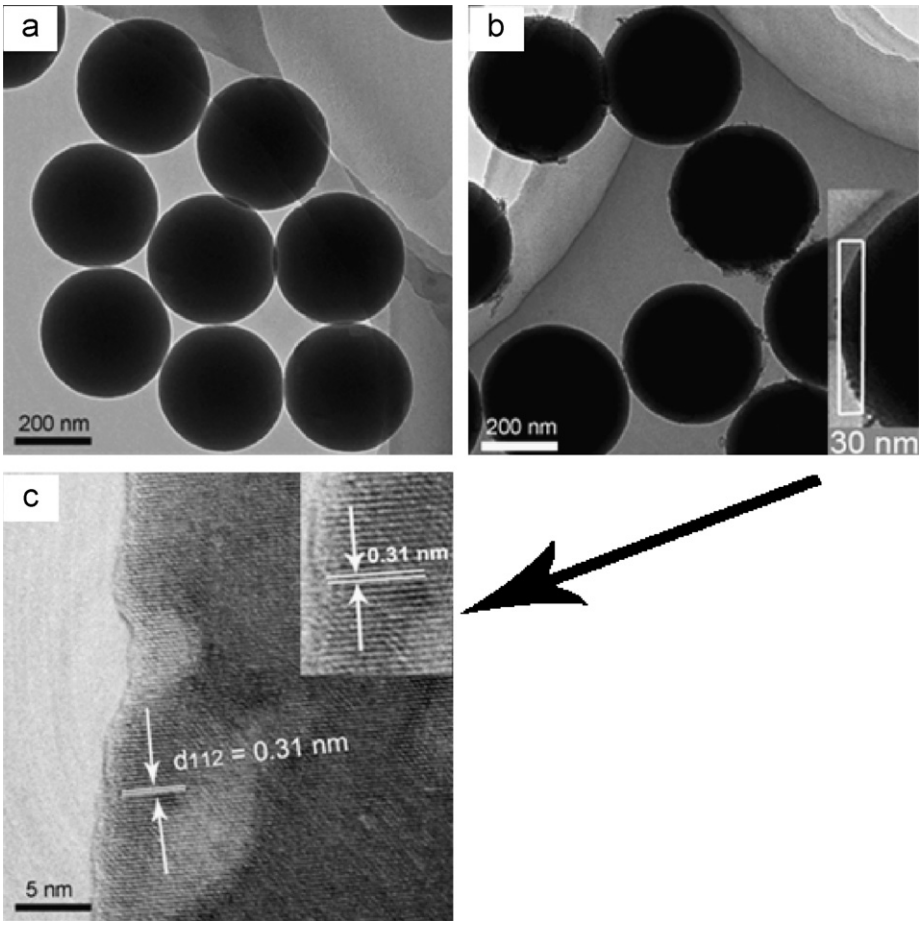

Fig. 3. TEM images of pure SiO_2 (a), $YNbO_4$:Eu^{3+}@SiO_2 (b), and HRTEM for $YNbO_4$:Eu^{3+}@SiO_2 coated with three times of phosphor layers (c).

(367 nm), $^7F_0 \rightarrow {}^5G_2$ (385 nm), $^7F_0 \rightarrow {}^5L_6$ (397 nm), $^7F_0 \rightarrow {}^5D_3$ (419 nm), $^7F_0 \rightarrow {}^5D_2$ (468 nm), respectively [32]. Upon excitation into the NbO_4^{3-} groups at 255 nm, not only the characteristic transition lines from the lowest excited $^5D_0$ but also those from higher energy levels ($^5D_1$) with weak intensities are observed (Fig. 5(b)). The emission of Eu^{3+} is dominated by the red $^5D_0$–$^7F_2$ hypersensitive transition, indicating that Eu^{3+} is located at a site without inversion symmetry [6,7]. For the $YNbO_4$:Tb^{3+}@SiO_2

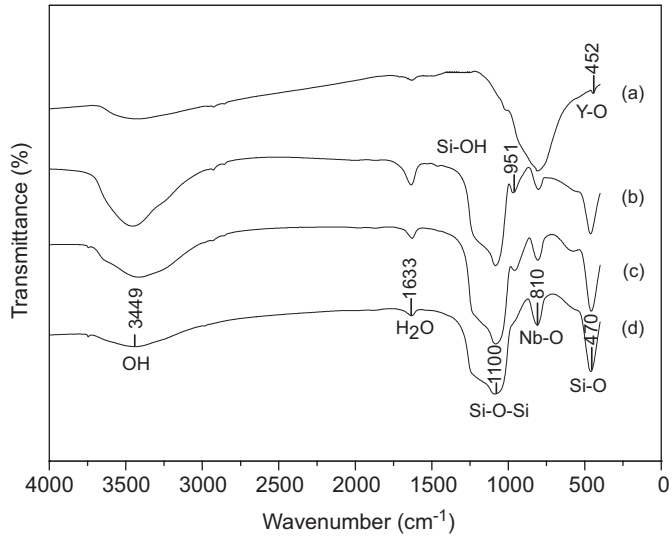

Fig. 4. FT-IR spectra for the 600 °C annealed pure $YNbO_4$ powder (a), SiO_2 (b), $YNbO_4$:Eu^{3+}@SiO_2 (c), and $YNbO_4$:Tb^{3+}@SiO_2 (d).

phosphor, the strong excitation band observed at 250 nm corresponds to the charge-transfer transitions within the $YNbO_4$ groups (Fig. 5(c)). No excitation peaks of Tb^{3+} from its $f \rightarrow f$ transitions can be detected because of their relatively low intensity with respect to that of $YNbO_4$ group. So it can be deduced that the excitation of Tb^{3+} is mainly caused by the energy transfer from NbO_4^{3-}. It should be noted that there are some difference between our spectrum and that in the paper [33]. Very small or almost non-broad band ascribed to NbO_4^{3-} is observed in the spectrum (Fig. 5(c)), while it is obvious in the previous paper's spectra. The difference in the excitation spectrum may be caused by the different examining temperature. Upon excitation into the NbO_4^{3-} at 250 nm, the obtained emission spectrum (Fig. 5(d)) contains characteristic emission of Tb^{3+} with the most prominent $^5D_4$–$^7F_5$ emission (544 nm) as well as other transitions. Furthermore, no emission from NbO_4^{3-} is detected, indicating an efficient energy transfer from NbO_4^{3-} to Tb^{3+}.

The representative decay curves for the luminescence of Eu^{3+} in the $YNbO_4$:Eu^{3+}@SiO_2 phosphors and Tb^{3+} in the $YNbO_4$:Tb^{3+}@SiO_2 phosphors are shown in Fig. 6. The decay curves for $^5D_0$–$^7F_2$ (612 nm) of Eu^{3+} and $^5D_4$–$^7F_5$ (544 nm) of Tb^{3+} can be well fitted into a double-exponential function as $I = A_1 \exp(-t/\tau_1) + A_2 \exp(-t/\tau_2)$

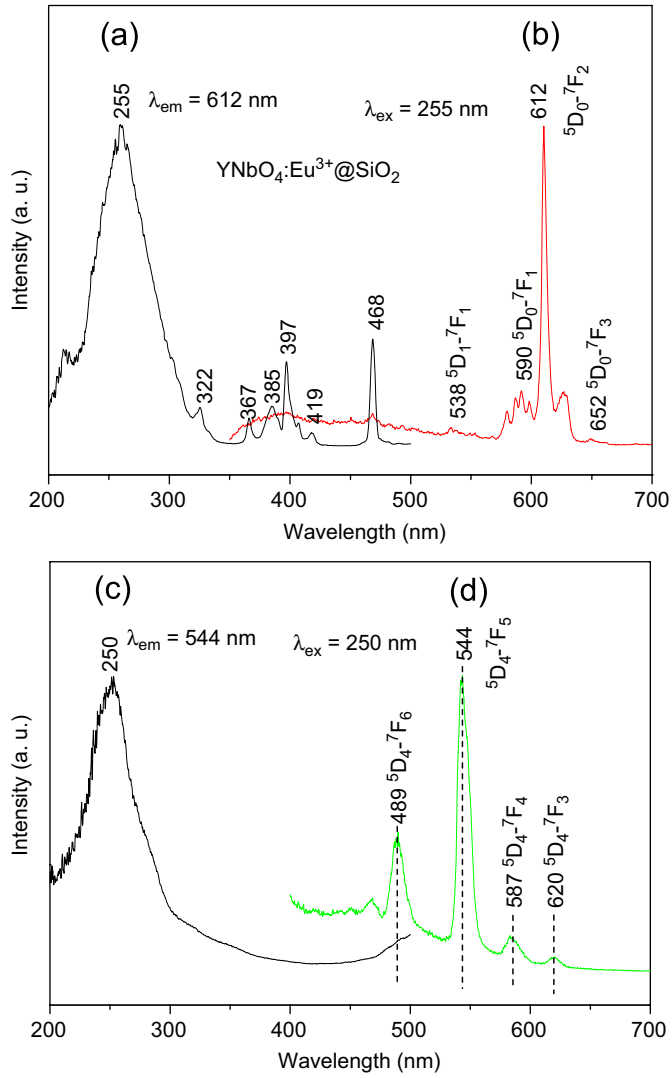

Fig. 5. Excitation spectra (a, c) and emission spectra (b, d) for $YNbO_4$:Eu^{3+}@SiO_2 and $YNbO_4$:Tb^{3+}@SiO_2.

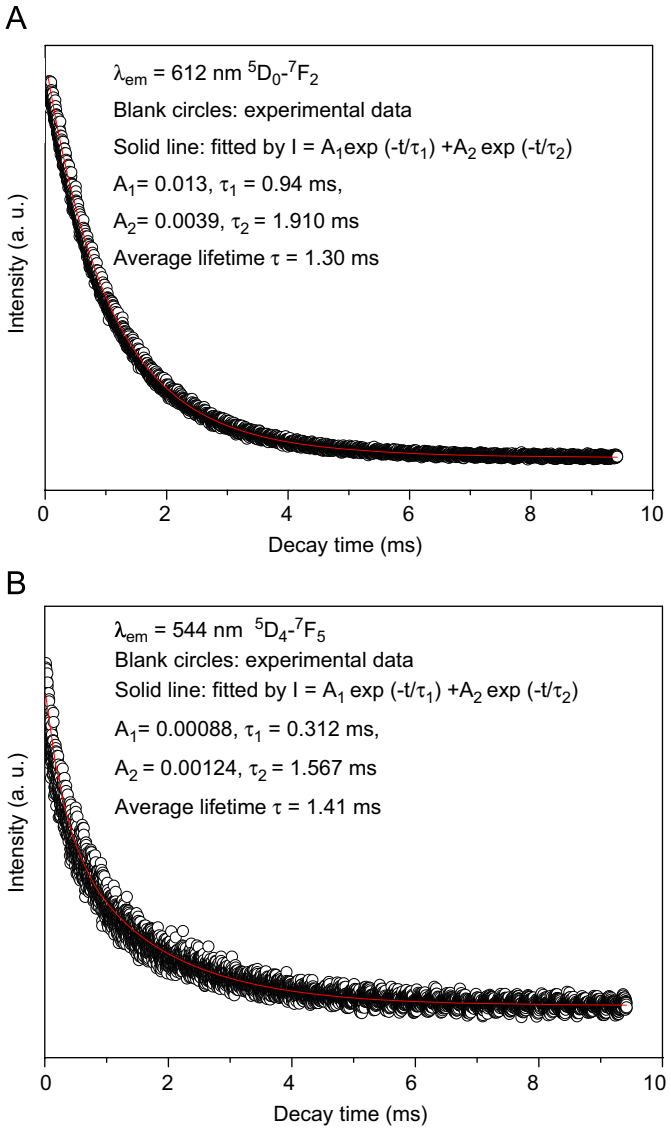

Fig. 6. Decay curves for the luminescence of Eu^{3+} in $YNbO_4$:Eu^{3+}@SiO_2 and Tb^{3+} in $YNbO_4$:Tb^{3+}@SiO_2 annealed at 600 °C.

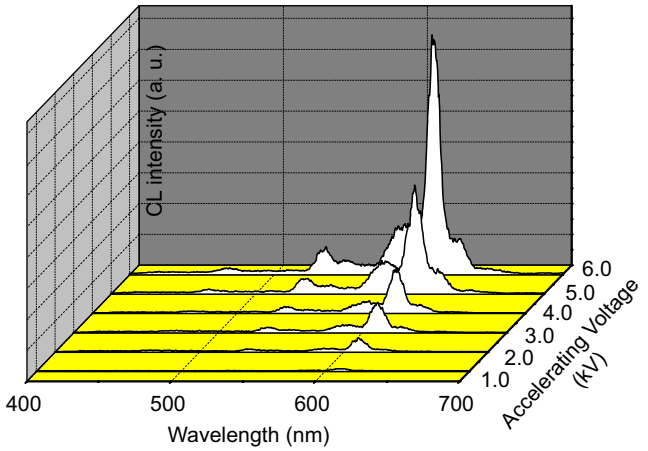

Fig. 7. The CL emission intensities of Eu^{3+} in $YNbO_4$:Eu^{3+}@SiO_2 as a function of accelerating voltage.

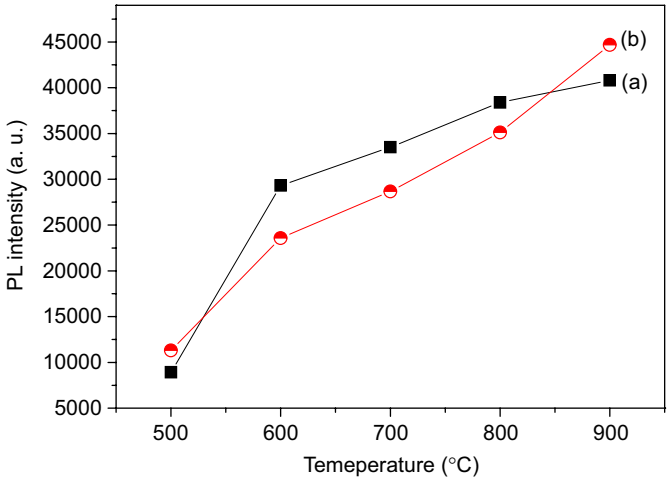

Fig. 8. The PL emission intensities of Eu^{3+} in $YNbO_4$:Eu^{3+}@SiO_2 (a) and Tb^{3+} in $YNbO_4$:Tb^{3+}@SiO_2 (b) as a function of annealing temperature.

(τ_1 and τ_2 are the fast and slow components of the luminescence lifetimes, A_1 and A_2 are the fitting parameters). The average lifetimes for $^5D_0$–$^7F_2$ (612 nm) of Eu^{3+} and $^5D_4$–$^7F_5$ (544 nm) of Tb^{3+} are determined by the formula as $\tau = (A_1\tau_1^2+A_2\tau_2^2)/(A_1\tau_1+A_2\tau_2)$, and the fitting results are shown in the Fig. 6 [34]. The respective average lifetimes for $^5D_0$–$^7F_2$ (612 nm) of Eu^{3+} and $^5D_4$–$^7F_5$ (544 nm) of Tb^{3+} are 1.30 and 1.41 ms, respectively. The double-exponential decay behavior of the activator is frequently observed when the excitation energy is transferred from the donor to acceptor [35].

Fig. 7 shows the CL spectra of $YNbO_4$:Eu^{3+}@SiO_2 under excitation of an electron beam (1–6 kV), which are well consistent with its corresponding PL spectra. As shown, only emissions from $^5D_0$–$^7F_{1,2,3,4}$ are observed, suggesting an efficient energy transfer from NbO_4^{3-} to Eu^{3+} as well as direct excitation of Eu^{3+} by the plasmas produced by the incident electrons. In addition, it can be clearly seen that the CL intensity increase with the increase of accelerating voltage from 1 to 6 kV. This can be attributed to the different penetration depth of electrons, which is determined by the energy of the electron beams.

3.3. *Effect of the treating conditions on the PL emission intensity*

Effect of annealing temperature on the PL emission intensity of the Eu^{3+} in $YNbO_4$:Eu^{3+}@SiO_2 and Tb^{3+} in $YNbO_4$:Tb^{3+}@SiO_2 is shown in Fig. 8. Obviously, the PL intensities all increase with increasing annealing temperature. This can be attributed to the enhanced crystallinity of the $YNbO_4$:Eu^{3+}/Tb^{3+}@SiO_2 phosphors (Fig. 1). Meanwhile, the components of impurities such as –OH, NO_3^-, $-CH_2$ have been markedly reduced. Therefore, the quenching effect on the luminescence by the vibrations of these impurities decreases, resulting in the increase of the emission intensity. Fig. 9 displays the effect of coating number on the PL intensity of the Eu^{3+} in $YNbO_4$:Eu^{3+}@SiO_2 and Tb^{3+} in $YNbO_4$:Tb^{3+}@SiO_2 phosphors. As shown, the PL intensity increases with increasing coating number, which can be due to increased thickness of $YNbO_4$:Eu^{3+}/Tb^{3+} shells on the SiO_2 cores. When the coating number is 5, the PL intensities of the obtained phosphors are 85% of that of pure $YNbO_4$:Eu^{3+} and 81% of pure $YNbO_4$:Tb^{3+} powders, respectively. It should be noted that the luminescent properties between the pure $YNbO_4$:Eu^{3+} powders and core–shell structured $YNbO_4$:Eu^{3+}@SiO_2 are similar except for a slight decrease of the emission intensity.

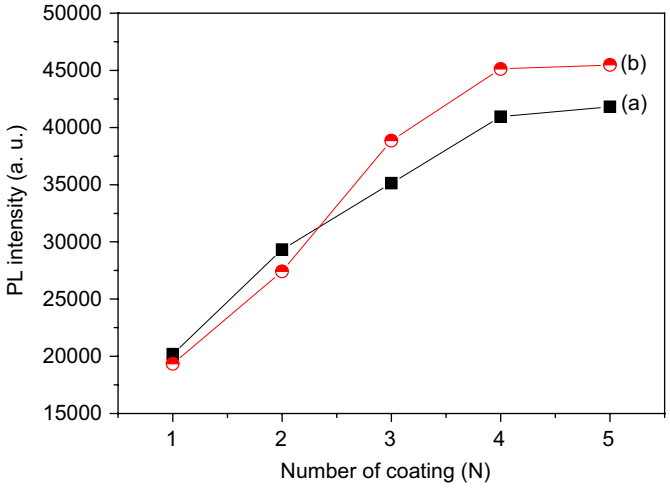

Fig. 9. The PL emission intensities of Eu^{3+} in Eu^{3+} in $YNbO_4$:Eu^{3+}@SiO_2 (a) and Tb^{3+} in $YNbO_4$:Tb^{3+}@SiO_2 (b) as a function of phosphor coating times.

4. Conclusions

A simple and effective sol–gel process has been developed to coat $YNbO_4$:Eu^{3+} and $YNbO_4$:Tb^{3+} phosphor layers on monodisperse spherical silica particles. The obtained core–shell structured $YNbO_4$:Eu^{3+}@SiO_2 and $YNbO_4$:Tb^{3+}@SiO_2 phosphors keep the spherical morphology, nanometer size and narrow size distribution. Under UV light and low-voltage electron beam excitation, the $YNbO_4$:Eu^{3+}@SiO_2 and $YNbO_4$:Tb^{3+}@SiO_2 phosphors exhibited strong luminescence. The PL intensity of the core–shell phosphors can be controlled by tuning the annealing temperature and the phosphor coating times. The obtained core–shell phosphors have potential applications in the luminescent fields.

Acknowledgments

This project is financially supported by the foundation of "Bairen Jihua" of Chinese Academy of Sciences, the MOST of China (2003CB314707, 2007CB935502), and the National Natural Science Foundation of China (NSFC 50572103, 20431030, 00610227).

References

[1] V. Suryanarayanan, A.S. Nair, R.T. Tom, J. Mater. Chem. 14 (2004) 2661.
[2] F. Caruso, Adv. Mater. 13 (2001) 11.
[3] W. Schartl, Adv. Mater. 12 (2000) 1899.
[4] S.J. Oldenberg, R.D. Averitt, S.L. Westcott, N.J. Halas, Chem. Phys. Lett. 288 (1998) 243.
[5] L.M. LizMarzan, M. Giersig, P. Mulvaney, Langmuir 12 (1996) 4329.
[6] M. Yu, J. Lin, Fang J. Chem. Mater. 17 (2005) 1783.
[7] M. Yu, J. Lin, Z. Wang, J. Fu, S. Wang, H.J. Zhang, Y.C. Han, Chem. Mater. 14 (2002) 2224.
[8] J.J. Schneider, Adv. Mater. 13 (2001) 529.
[9] C.J. Zhong, M.M. Maye, Adv. Mater. 13 (2001) 1507.
[10] M.S. Fleming, T.K. Mandal, D.R. Walt, Chem. Mater. 13 (2001) 2210.
[11] R.A. Caruso, M. Antonietti, Chem. Mater. 13 (2001) 3272.
[12] F. Caruso, H. Lichtenfeld, H. Mohwald, J. Am. Chem. Soc. 120 (1998) 8523.
[13] F. Caruso, R. Caruso, H. Mohwald, Science 282 (1998) 1111.
[14] Z.H. Jiang, C.Y. Liu, J. Phys. Chem. B 107 (2003) 12411.
[15] H. Sertchook, D. Avnir, Chem. Mater. 15 (2003) 1690.
[16] M. Giersig, T. Ung, L.M. Liz-Marzan, P. Mulvaney Adv. Mater. 9 (1997) 570.
[17] S.R. Hall, S.A. Davis, S. Mann, Langmuir 16 (2000) 1454.
[18] P. Schuetzand, F. Caruso, Chem. Mater. 14 (2002) 4509.
[19] I. Sondi, T.H. Fedynyshyn, R. Sinta, E. Matijevic, Langmuir 16 (2000) 9031.
[20] M.I. Martinez-Rubio, T.G. Ireland, G.R. Fern, J. Silver, M.J. Snowden, Langmuir 17 (2001) 7145.
[21] X. Jing, T.G. Ireland, C. Gibbons, D.J. Barber, J. Silver, A. Vecht, G. Fern, P. Trogwa, D. Morton, J. Electrochem. Soc. 146 (1999) 4546.
[22] Y.D. Jiang, Z.L. Wang, F. Zhang, H.G. Paris, C.J. Summers, J. Mater. Res. 13 (1998) 2950.
[23] A. Celikkaya, M. Akinc, J. Am. Ceram. Soc. 73 (1990) 2360.
[24] S.H. Cho, J.S. Yoo, J.D. Lee, J. Electrochem. Soc. 145 (1998) 1017.
[25] W. Stöber, A. Fink, E. Bohn, J. Colloid Interf. Sci. 26 (1968) 62.
[26] P. Jiang, J.F. Bertone, K.S. Hwang, V.L. Colvin, Chem. Mater. 11 (1999) 2132.
[27] J. Li, C.M. Wayman, J. Am. Ceram. Soc. 80 (1997) 803.
[28] L.H. Brixner, Mater. Chem. Phys. 16 (1987) 253.
[29] M.P. Pechini, US Patent, 1967, 3330697.
[30] L.S. Birks, H. Friedman, J. Appl. Phys. 17 (1946) 687.
[31] A.K. Pradhan, R.N.P. Choudhary, Phys. Status Solidi B 143 (1987) K161.
[32] C.X. Li, Z.W. Quan, J. Yang, P.P. Yang, J. Lin, Inorg. Chem. 46 (2007) 6329.
[33] P. Boutinaud, E. Cavalli, M. Bettinelli, Phys.: Condens. Matter 19 (2007) 386230.
[34] S. Mukarami, H. Markus, R. Doris, M. Makato, Inorg. Chim. Acta 300 (2000) 1014.
[35] C. Hsu, R.C. Poweh, J. Lumin. 10 (1975) 273.